A Method of Arrival Angle Optimization in Single-Station Positioning Based on Statistical Features

Ting Li [1] , **Tongxin Liu** [2,*] , **Xuehai Yang** [1] , **Guobin Yang** [2] , **Chunhua Jiang** [2] **and Chongzhe Lao** [2]

[1] Southwest China Institute of Electronic Technology, Chengdu 610036, China; liting860512@163.com (T.L.); yangmxh@163.com (X.Y.)
[2] School of Electronic Information, Wuhan University, Wuhan 430072, China; gbyang@whu.edu.cn (G.Y.); chuajiang@whu.edu.cn (C.J.); krislao@whu.edu.cn (C.L.)
[*] Correspondence: tongxin_liu@whu.edu.cn; Tel.: +86-27-6877-8049

Abstract: Aiming to mitigate the substantial dispersion in arrival angle estimation due to colored and white noise interference, which may seriously affect the accuracy of short-wave single-station positioning, this paper introduces an approach to optimizing angles based on the statistical features. By utilizing the extraction of the main peak area of the probability density distribution of the measured angle, as well as the two-dimensional Gaussian fitting and confidence ellipse bounding, the angle measurement results affected by colored noise interference and the noise points with large deviations can be sequentially filtered out. Combining experimental scenarios and confirmed by actual measurement data, the dispersion of arrival angle estimation results has been significantly constrained, and, correspondingly, the positioning accuracy has also been significantly improved by about 3%.

Keywords: short-wave single-station positioning; arrival angle optimization; accuracy evaluation

1. Introduction

Short-wave single-station positioning technology has attracted much attention and extensive research due to its important engineering practical value. It usually utilizes an estimation of the signal arrival angle, combined with ionospheric state information, and uses ray tracing to determine the location of the radiation source. Although the state of the ionosphere can be obtained through various means, it is precisely because the ionosphere is a disperse channel which varies temporally and spatially [1], with the interference of noise, that the quality of the received signal is often degraded. As a result, the estimation of the angle of arrival (AOA) can be greatly influenced, causing the dispersion of positioning points [2].

Without doubt, accurately estimating the angle of arrival is essential for describing high-frequency channel properties, and is significant in short-wave single-station positioning technology. To achieve this, a typical sensor array is always utilized. Moreover, relative two-dimensional (2-D) direction of arrival (DOA) methods can provide the angle of arrival estimation [3]. Various techniques have been proposed for this purpose [4]. Among them the maximum likelihood estimator provides the optimum parameter estimation, but its computational complexity restricts its practical use. Conventional subspace techniques, such as Multiple Signal Classification (MUSIC) [5] and Estimation of Signal Parameters via Rotational Invariance Techniques (ESPRIT) [6], are widely used for 2-D DOA methods because of their low computational cost and reliable performance. These methods estimate

the signal and noise subspaces by utilizing the eigen-decomposition of the covariance matrix. These methods are efficient in computation, but, due to the sensitivity of colored noise [7] and the dispersion caused by white noise, they could not provide sufficient stability and accuracy. In 1973, Brennan and Reed proposed the space–time adaptive signal processing techniques [8], which mitigated the limitations of array structures and improved noise resistance. The conventional spatial spectrum DOA estimation might not fully utilize the valuable information of the signal, since it ignores the signal's time characteristics [9]. Therefore, it is necessary that we introduce the proper processing to overcome colored interference and converge the dispersion of positioning points under the influence of white noise.

To address the problem of scattered positioning points caused by the dispersion of arrival angles, this paper proposes an optimal selection method for arrival angles based on statistical means and a sequence of angle measurements over a specific period of time. It is mainly based on the distribution of the probability density function of angle measurement results, and performs a two-dimensional Gaussian fitting of the azimuth-elevation angle for its main peak area. Thereby, the angle screening region can be determined based on the confidence level. This method can overcome the short-term drift of the angle estimation results caused by colored noise and also counteract the dispersion caused by white noise. The experiment of this method was conducted using the Wuhan Ionospheric Sounding System (WISS) and an L-shaped array. Its effectiveness was also verified through a positioning program. The positioning results before and after optimization were displayed and compared with the method of using the simple mean of angle measurement results. The results indicate that the dispersion of angles has been effectively overcome, and the positioning has also achieved higher accuracy. It should have considerable engineering practical reference value for the single-station positioning of short-wave radiation sources for quasi-static targets.

The following sections of this paper are organized as follows: Section 2 presents the experiment scenarios and preconditions; Section 3 describes the principle of angle optimization method combining the measurement data; Section 4 presents the positioning results and analysis; and Section 5 is the conclusion.

2. Experiment Scenarios and Preconditions

2.1. Experimental Scenario

To verify the angle optimization method mentioned in this paper and obtain accurate ionospheric patterns and states, the Ionosphere Laboratory at Wuhan University constructed an experimental scenario as shown in Figure 1. It includes a transmitting station located in Wuhan (114.37°E, 30.54°N), Hubei, equipped with a transmitter system. In Kunshan (120.95°E, 31.50°N), Jiangsu, a single-channel receiving system is configured to cooperate with the transmitting station to conduct ionospheric oblique incidence sounding to obtain an ionospheric state. And a multi-channel receiving system is also configured to cooperate with an L-shaped antenna array for the angle of arrival estimation at the same venue. The ionospheric sounding and angle of arrival estimation experiments are conducted in a time-sharing manner, using the shared transmission source. This can be regarded as a slowly changing target scenario, which facilitates the evaluation of the arrival angle convergence and positioning performance.
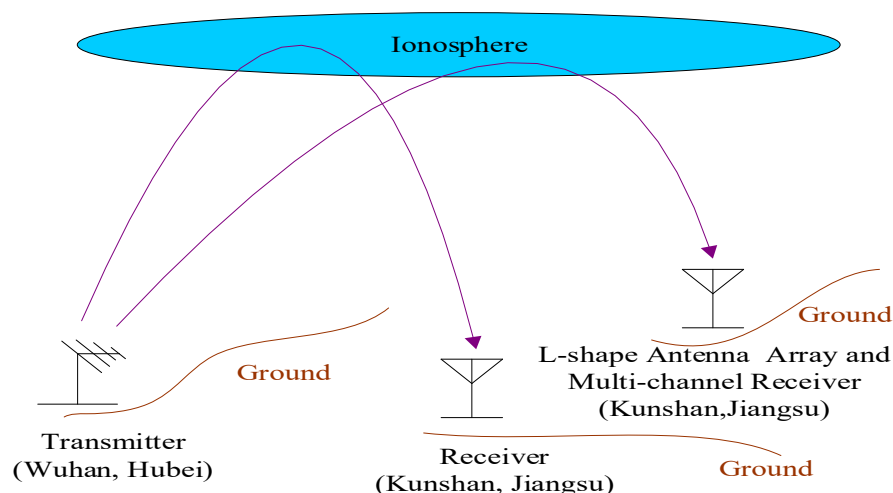
Figure 1. The experimental scenario includes a transmitting station and two receiving stations. The transmitting station cooperates with two receiving stations to analyze the ionospheric state and estimate the angle of arrival. An L-shaped directional antenna array was applied.

2.2. Ionospheric State Acquisition

For the oblique incidence sounding method of the ionosphere, based on general principles, it is plausible to treat the ionospheric channel as a linear time-variant system, described with its bitemporal ionospheric response (BTIR) function. It can be approximated from the cross-correlation function of the transmitted signal and the received signal [10–12]. The data acquired by the WISS were also analyzed using the BTIR function to obtain the oblique ionograms, which can provide important information such as the group range and reflection virtual height of signal echoes [13].

Based on the system characteristics of the WISS, the typical sounding parameters can be seen in the Table 1:

Table 1. Typical sounding parameters of WISS.

Parameters	Value
Transmitting power	500 W
Frequency range	2–20 MHz
Waveform mode	Biphase modulation
Code system	Complementary code
Code sequence length	16 bits
Bit duration	25.6 μs
Duty cycle	5%
Downconversion decimation factor	32

Thus, a typical ionogram of oblique incidence sounding between the experimental transmitter and receiver station can be shown in Figure 2. Obviously, the echo trace contains multiple modes, including the F2 layer and E/Es (sporadic E) layer reflection signals. The maximum available frequency of the F2 layer is below 10 MHz, and the group range is above 700 km, while the maximum available frequency of E/Es exceeds 10 MHz, and the echo group distance is below 700 km. It can be used to determine the propagation mode of signals in actual measurements and the theoretical elevation angle value, providing important reference for determining the reflection virtual height and evaluating the angle optimization effect during the positioning process.
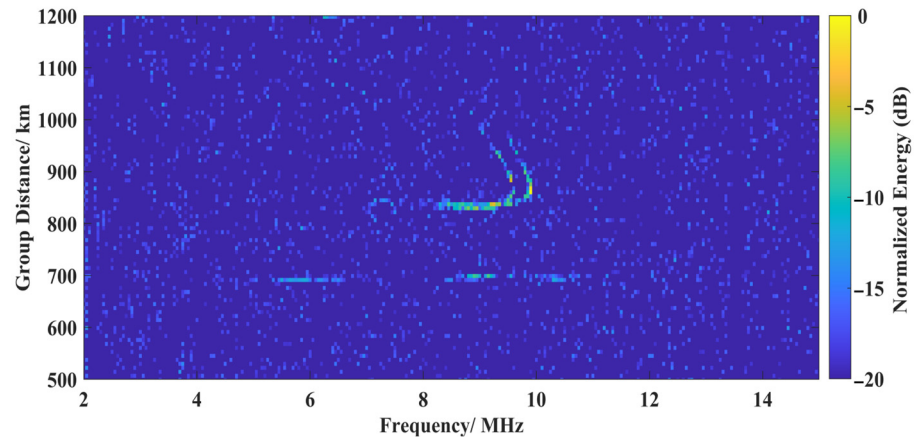
Figure 2. Typical oblique ionogram at LT 08:26, 15 August 2022.

2.3. Calculation of Theoretical Arrival Angle

As shown in Figure 3, for a distribution of transmitting and receiving stations that are relatively close, with the equivalent path theory, the transmitting path of the radio signal and the ground distance between the receiver and transmitter can create an approximate isosceles triangle.
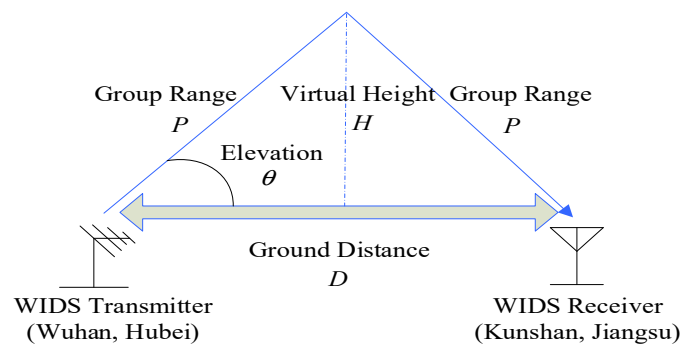
Figure 3. Simplified signal propagation model based on the equivalent path theorem.

Based on the latitude and the longitude of the two locations, the ground distance D is obtained by calculating as follows:

$$D = R \cdot \arccos(\sin(\varphi_T)\sin(\varphi_R) + \cos(\varphi_T)\cos(\varphi_R)\cos(\alpha_T - \alpha_R)) \tag{1}$$

where φ_T and φ_R are the latitude of the transmitting and receiving stations, respectively. α_T and α_R are the longitudes. R is the radius of the Earth. In the experimental scenario of this paper, the value of D is 636.19 km. Similarly, for the azimuth between two locations, it can also be calculated based on the latitude and longitude:

$$\beta = \arctan\left(\frac{\sin(\alpha_T - \alpha_R) \cdot \cos(\varphi_T)}{\cos(\varphi_R) \cdot \sin(\varphi_T) - \sin(\varphi_R) \cdot \cos(\varphi_T) \cdot \cos(\alpha_T - \alpha_R)}\right) \tag{2}$$

For the experimental scenario in this paper, the theoretical azimuth should be 262.00°.

And, according to the geometry presented in Figure 3, the ground distance D can also be calculated from the group range P, the reflection virtual height H, and the elevation angle θ. It can be expressed as follows:

$$D = P \cdot \sin(\theta) = 2H / \tan(\theta) \tag{3}$$

As the distance between the transmitting and receiving stations in the experiment is not very far, the effect of the Earth curved surface is ignored here for ease of calculation. But, in practical applications at longer distances, the curvature of the Earth surface should be considered in order to ensure the position accuracy.

And, due to the inability to obtain the signal propagation group distance in single-station positioning applications, positioning is usually based on angle measurement results (β, θ) and ionospheric reflection virtual height H. (In cases where an accurate H cannot be obtained, ionospheric models are usually used for ray tracing. In order to verify the effectiveness of angle optimization, this paper obtained accurate H values through ionospheric sounding.)

2.4. Estimation of Arrival Angle

For the estimation of the signal arrival angle, a multi-channel receiving system, especially an L-shaped antenna array, is adopted. Compared to a uniform circular array, an L-array has lower requirements for the field and is easier to utilize to achieve a higher installation accuracy due to its composition of two linear arms. The multi-channel system receives radiation signals from the transmitting station, which do not have specific requirements. In the experiment, a single tone signal was used. The L-shaped array as illustrated in Figure 4, consists of N identical isotropous antennae placed on the X-axis and M identical isotropous antennae placed on the Y-axis. This scenario employs a nine-element L-array, where $N = M = 9$. The spacing between adjacent columns and rows is dx and dy ($dx = dy = 10$ m), respectively. In the experiment, the direction of the x-axis pointing north is the starting point of the azimuth angle, and the clockwise direction is the positive.
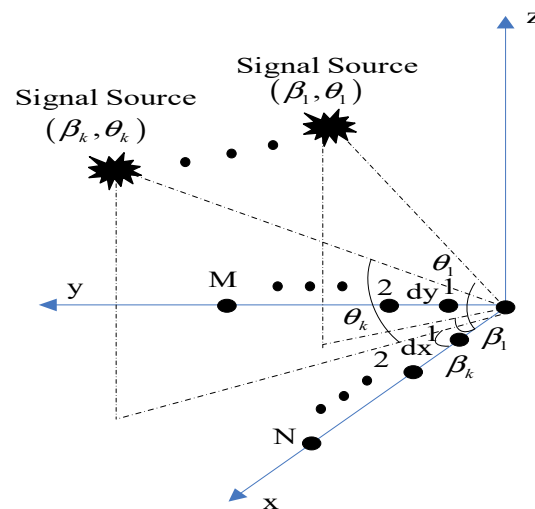
Figure 4. The L-shape array configuration.

Supposing that there are k narrow-band sources, $s_i(t)(i = 1, \cdots, k)$, with the same wavelength λ impinging on the array from directions $(\beta_1, \theta_1), (\beta_2, \theta_2), \cdots, (\beta_k, \theta_k)$, where β_i and θ_i denote the azimuth and the elevation angle of arrival of the *ith* signal, respectively. Then, the array steering vector can be expressed as follows:

$$a(\beta_i, \theta_i) = a_y(\beta_i, \theta_i) \otimes a_x(\beta_i, \theta_i), i = 1, 2, \cdots, k \tag{4}$$

$$a_x(\beta_i, \theta_i) = [1, \exp(j2\pi dx \cos\beta_i \sin\theta_i/\lambda), \cdots, \exp(j2\pi(N-1)dx \cos\beta_i \sin\theta_i/\lambda)]^T \tag{5}$$

$$a_y(\beta_i, \theta_i) = [1, \exp(j2\pi dy \sin\beta_i \sin\theta_i/\lambda), \cdots, \exp(j2\pi(M-1)dy \sin\beta_i \sin\theta_i/\lambda)]^T \tag{6}$$

$\otimes$ is represents the Knorr product.

In this paper, the 2-D MUSIC algorithm is employed. Its basis is to construct an appropriate pseudo spectrum. This pseudo spectrum is a function of the array steering vector and the noise or signal subspace, which is constructed by appropriate eigenvalues of the array correlation matrix [14]. By using the orthogonal characteristics of eigenvectors in the signal and noise subspaces, the MUSIC algorithm pseudo spectrum with the L-shape array is given by the following expression:

$$P_{MUSIC\_L} = \frac{1}{\left[a_y(\beta,\theta) \otimes a_x(\beta,\theta)\right]^H E_N E_N^H \left[a_y(\beta,\theta) \otimes a_x(\beta,\theta)\right]} \tag{7}$$

where E_N is the noise subspace of the covariance matrix of the array signal $[s_1(t), \cdots, s_k(t)]^T$. According to Formula (7), the original elevation and azimuth angles can be computed through the 2-D search.

3. Principle of Angle Optimization Method

As per the spatial spectrum principle, the angle of arrival should be time-independent and determined by the sites of the transmitter and the receiver [15]. However, due to the numerous interference signals in the short-wave band and the effect of the occasional colored noise or white noise, the results of the arrival angle estimation are usually scattered. Nevertheless, in general, for effective measurement frequencies, colored noise is generally short-lived (the frequency with persistent colored interference will be considered as ineffective and not suitable for processing), while white noise exhibits typical statistical patterns. Therefore, this paper proposes an optimal solution based on the characteristics of probability distribution and statistical features. The following will provide a specific description based on the measurement data from 15 August 2022.

3.1. Colored Interference Filtering Based on Probability Density Function

The experiment used three frequencies of 10.4, 12.1, and 10.2 MHz, and obtained 3200, 2269, and 2869 effective angle of arrival estimation pairs at 08:42–08:54, 08:57–09:06, and 09:27–09:37 local time (LT), respectively. In the respective time periods, as a slowly changing medium, the evolution process of the ionosphere was ignored. With a resolution of 0.1°, the distribution of measurement results can be shown as Figure 5. (Obviously, there is a certain overall deviation between the estimated azimuth and the theoretical value, which may be due to the systematic error in the baseline pointing calibration of the antenna array or the Ionospheric tilt. However, this does not affect the evaluation of dispersion constraints in this paper.)
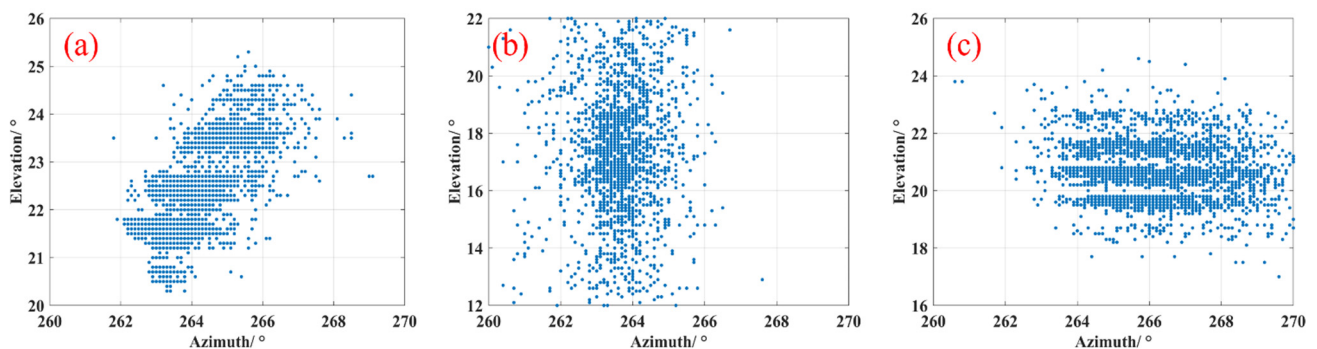
Figure 5. Arrival angle estimation result: (**a**) distribution of 10.4 MHz signal estimation results; (**b**) distribution of 12.1 MHz signal estimation results; and (**c**) distribution of 10.2 MHz signal estimation results.

Obviously, although the angle measurement results of the 12.1 MHz signal have a large dispersion, they exhibit a central divergent distribution. Differently, the 10.4 and 10.2 MHz signals are clearly divided into multiple groups. For the 10.4 MHz signal, it can be roughly divided into three large groups, with the azimuth angle in [262°, 265°] and the elevation angle in [21°, 22°]; the azimuth angle in [263°, 265°] and the elevation angle in [22°, 23°]; and the azimuth angle in [264°, 266.5°] and the elevation angle in [23°, 25°]. A smaller group is located below the elevation of 21°. Similarly, the arrival angle of a 10.2 MHz signal can also be divided into four groups based on the elevation as [19°, 20°], [20°, 21°], [21°, 22°], and [22°, 23°]. Such a grouping dispersion can be considered as a form of colored noise interference when the hardware platform is consistent.

Obviously, this kind of interference is short-term and time-varying; otherwise, the clustering is difficult to form. Thus, the interfered angle measurement results can be filtered out according to the probability distribution of the angle measurement results. (Compared to traditional clustering methods, it can more conveniently filter out the interference of colored noise and achieve a better focusing on the results caused by white noise.) Therefore, the corresponding probability density distribution for the arrival angle distribution shown in Figure 5 can be obtained as in Figure 6:
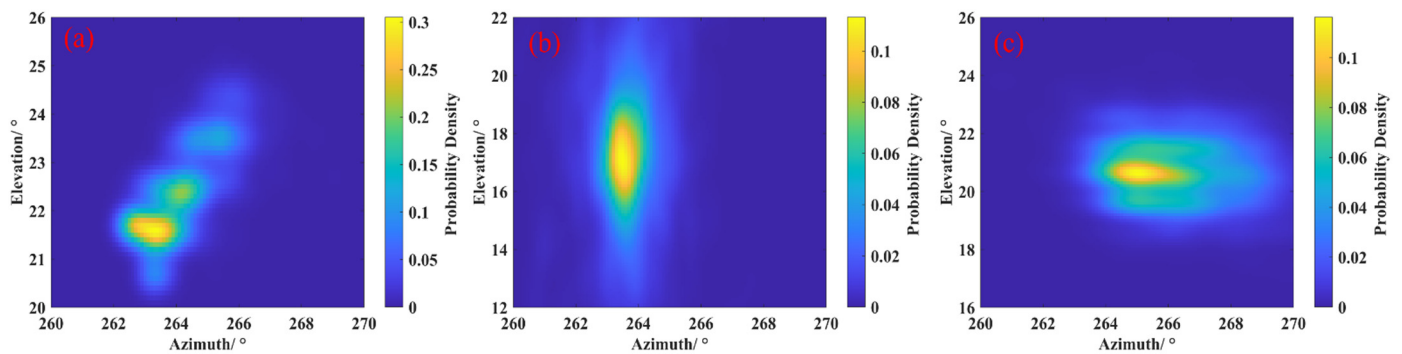
Figure 6. Probability density distribution of arrival angle: (**a**) probability density distribution of 10.4 MHz signal; (**b**) probability density distribution of 12.1 MHz signal; and (**c**) probability density distribution of 10.2 MHz signal.

Significantly, the probability density distribution of the measurement results has a unimodal form; thus, the filtering of colored noise interference results can be achieved by selecting the angle estimation results of the probability density main peak region. For the determination of the main peak area, this paper adopts a strategy of selecting a 2° neighborhood range centered on the maximum probability density. Hence, according to Figure 6, the main peak region results for frequency can be obtained as shown in Figure 7, and the corresponding highest probability density points are (263.4°, 21.7°), (263.6°, 17.2°), and (265.1°, 20.7°).

It can be seen that, although there is a slight difference in the maximum probability density of the three frequency estimation results, the overall distribution is similar to a Gaussian distribution. It implies that, when the influence of colored noise is filtered, the arrival angle estimation results are mainly affected by white noise, and should have similar statistical characteristics.
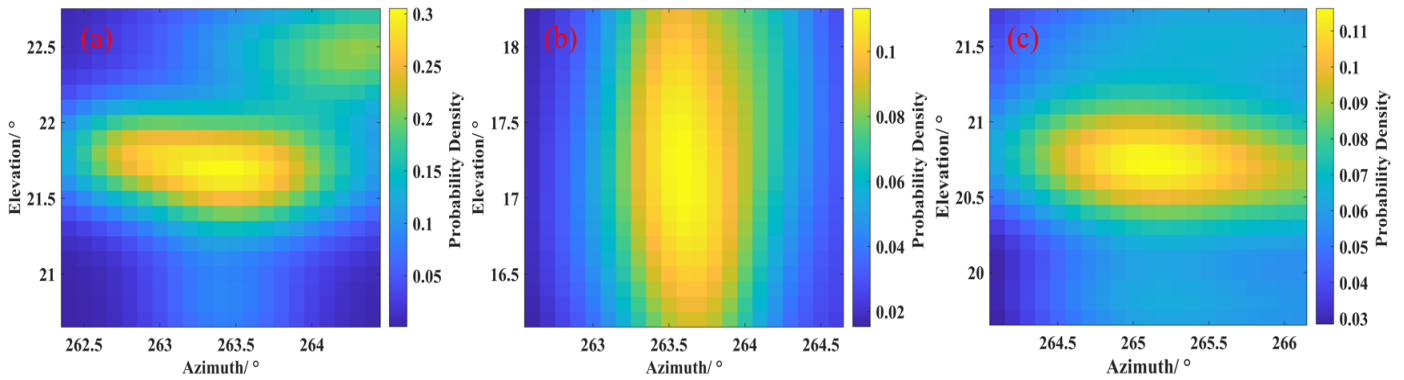
Figure 7. Extraction results of probability density main peak region: (**a**) main peak region of 10.4 MHz signal; (**b**) main peak region of 12.1 MHz signal; and (**c**) main peak region of 10.2 MHz signal.

3.2. Angle Selection Based on Two-Dimensional Gaussian Fitting and Confidence Interval

To further optimize the angle, this paper performed normalized 2-D Gaussian fitting on the main peak regions of the probability density functions of each frequency. Based on the Gaussian distribution center (β_0, θ_0), the variances σ_β and σ_θ, and the covariance of the two axes $\sigma_{\beta\theta}$, the fitting results for each frequency can be obtained according to Equation (8), as shown in Figure 8.

$$f(\beta, \theta) = \exp\left(-\frac{1}{2}\begin{pmatrix}\beta - \beta_0 \\ \theta - \theta_0\end{pmatrix}^T \Sigma^{-1}\begin{pmatrix}\beta - \beta_0 \\ \theta - \theta_0\end{pmatrix}\right) \tag{8}$$

where Σ is the covariance matrix:

$$\Sigma = \begin{bmatrix}\sigma_\beta^2 & \sigma_{\beta\theta} \\ \sigma_{\beta\theta} & \sigma_\theta^2\end{bmatrix} \tag{9}$$
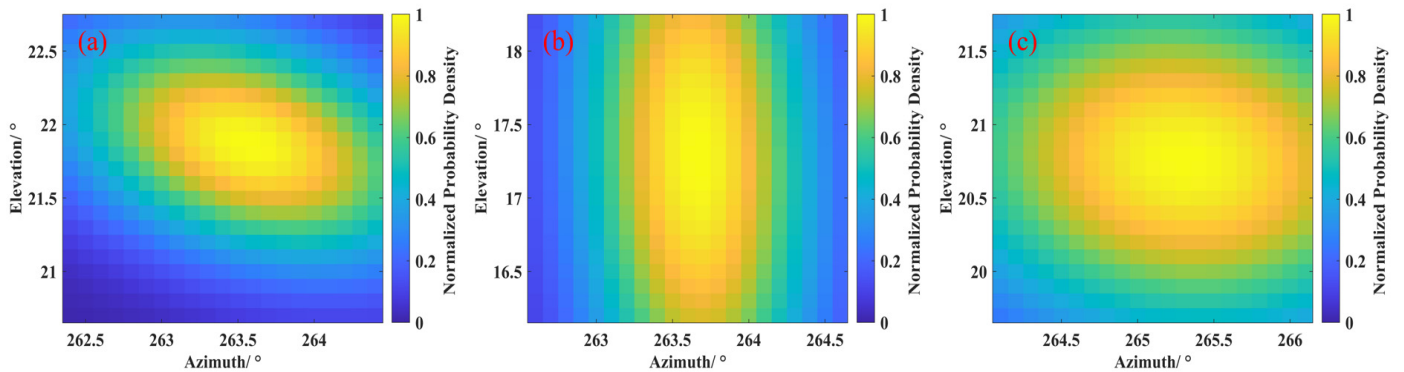
Figure 8. Normalized Gaussian fitting of probability density: (**a**) fitting result of 10.4 MHz signal; (**b**) fitting result of 12.1 MHz signal; and (**c**) fitting result of 10.2 MHz signal.

The inclination angle of the principal axis can be calculated as follows:

$$\psi = \frac{1}{2}\tan^{-1}\left(\frac{2\sigma_{\beta\theta}}{\sigma_\beta^2 - \sigma_\theta^2}\right) \tag{10}$$

Based on Equation (9), the eigenvalues of Σ can be calculated as $\lambda_\beta = \lambda_1$ and $\lambda_\theta = \lambda_2$.

$$\Sigma \mathbf{v}_i = \lambda_i \mathbf{v}_i, i = 1, 2 \tag{11}$$

where $\mathbf{v}_i$ are the eigenvectors.

And, when a confidence level η is given, the two axis lengths of its confidence ellipse can be calculated as follows:

$$a = \sqrt{\lambda_\beta} \cdot \sqrt{-2\ln(1-\eta)}, b = \sqrt{\lambda_\theta} \cdot \sqrt{-2\ln(1-\eta)} \tag{12}$$

From this, the confidence ellipse equation can be obtained as follows:

$$\begin{cases} \beta' = a\cos(t)\cos(\psi) - b\sin(t)\sin(\psi) \\ \theta' = a\cos(t)\sin(\psi) + b\sin(t)\cos(\psi) \end{cases}, t \in [0, 2\pi] \tag{13}$$

The angle selection criteria can be determined as follows:

$$\frac{[(\beta - \beta_0)\cos(\psi) + (\theta - \theta_0)\sin(\psi)]^2}{a^2} + \frac{[-(\beta - \beta_0)\sin(\psi) + (\theta - \theta_0)\cos(\psi)]^2}{a^2} \leq 1 \tag{14}$$

Consequently, when the selected confidence level is 0.9, the accepted measured arrival angle values between the straight ellipse and its interior can be obtained as shown in Figure 9. The corresponding number of accepted azimuth–elevation pairs are 138, 123, and 238, with ratios of 4.31%, 5.43%, and 8.30%. Although angle optimization has eliminated most of the results, it can still ensure an average of more than 10 outputs per minute without affecting the timeliness of long-range short-wave positioning.
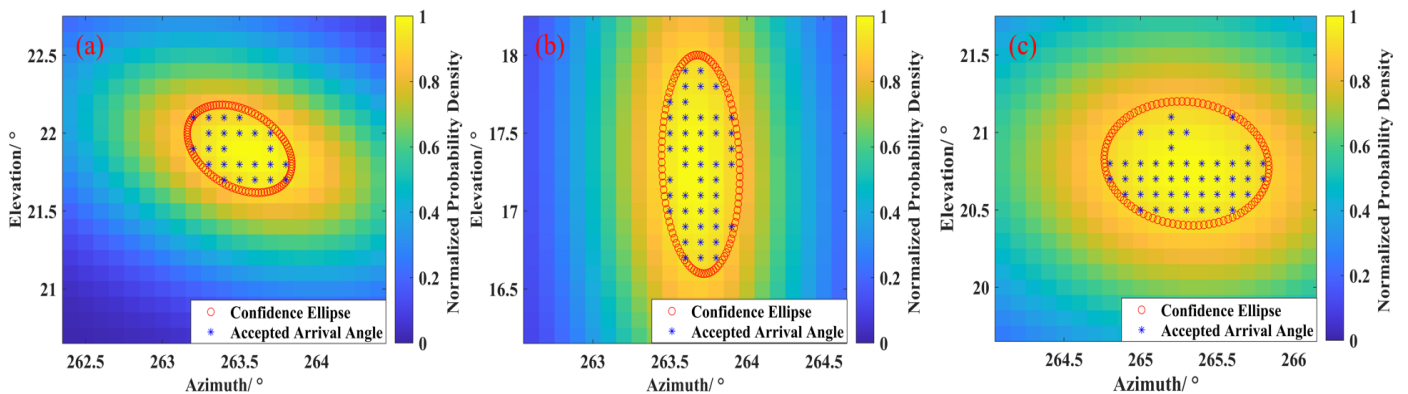
Figure 9. Distribution optimal accepted arrival angles: (**a**) accepted arrival angles of 10.4 MHz signal; (**b**) accepted arrival angles of 12.1 MHz signal; and (**c**) accepted arrival angles of 10.2 MHz signal.

It should be noted, at a higher level of confidence, there is a lower number of acceptable angles which may affect the real-time performance of positioning, especially in tracking moving targets. In practice, confidence levels should be set according to real-time requirements. But it can also be expected that a lower confidence level will inevitably lead to a larger scattering range of angles and positioning points.

4. Positioning Results and Analysis

To verify the constraint effectiveness of angle optimization on single-station positioning dispersion, the ionospheric oblique sounding ionograms were used for the pattern discrimination of signal propagation and the determination of the reflection virtual heights. To ensure the accuracy of obtaining ionospheric state information, oblique incidence soundings were conducted twice at LT 08:36 and 09:16, 15 August 2022, respectively, close to the arrival angle estimation period. The obtained ionograms are shown in Figure 10:
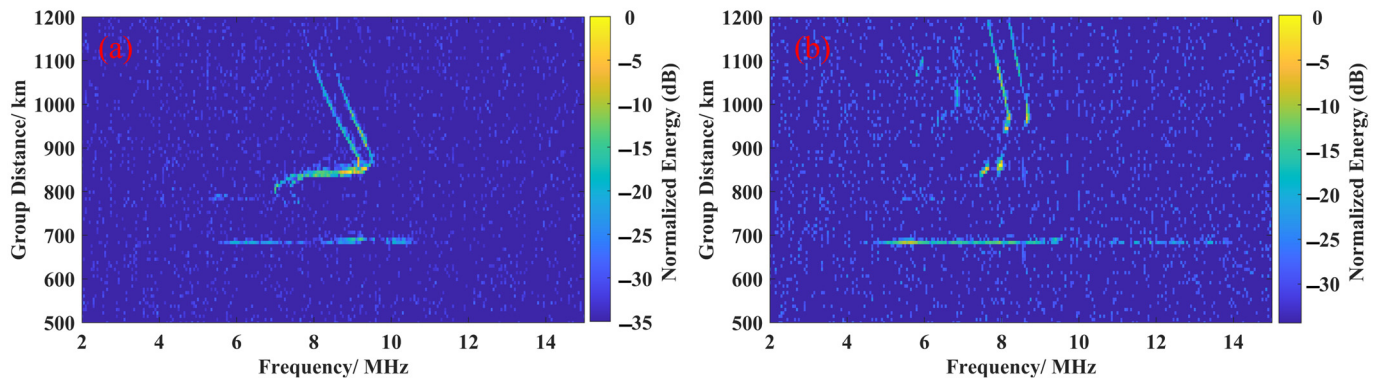
Figure 10. Oblique ionograms of arrival angle estimation period: (**a**) ionogram of LT 8:36, 15 August 2022; and (**b**) ionogram of LT 9:16, 15 August 2022.

It can be seen that the sounding ionograms reflects two modes of propagation: F-layer propagation and Es layer propagation. The maximum available frequency of the F-layer reflection is less than 10 MHz; thus, the three frequencies used for the angle of arrival estimation should only propagate through the Es layer. In addition, this Es layer should be in the development stage, and its critical frequency gradually increases with time. After LT 09:16, it can even reflect 14 MHz signals at the distance of the experimental scene in this paper. By measuring the ionization diagram, it can be determined that the propagation group distance of 10.2 and 10.4 MHz signals is 679.68 km, corresponding to a reflection virtual height of 119.61 km. The propagation group distance and reflection virtual height of the 12.1 MHz signal are 675.84 km and 114.04 km. The corresponding elevation angles are 20.61° and 19.72°. Based on this, the root mean square error (RMSE) before and after angle optimization can be obtained as Table 2, which can evaluate the improvement effect on accuracy. Where β_{or} and θ_{or} are the original estimated azimuth and elevation angle, β_{opt} and θ_{opt} are the optimized ones. The accuracy of the optimal values for the arrival angles of the three frequencies has significantly improved compared to the original measurement results. The RMSE of azimuth has been reduced 0.81°, 0.25°, and 1.28°, respectively. The reductions in RMSE in the elevation angles are 0.79°, 1.03°, and 0.90°.

It should be noted that, in order to demonstrate the convergence effect of angle optimization on the dispersion of positioning results, this paper only estimates and processes the arrival angle of the echo signal of the Es layer. For the more common multi-layer reflected waves, array signal processing methods can be used for multi-target estimation. As long as the arrival angle measurement results are correct, the preferred method in this paper should also be able to distinguish patterns and impose dispersion constraints based on the probability density and confidence level.

Table 2. RMSE statistics of angle estimation results.

Frequency	RMSE (β_{or})	RMSE (β_{opt})	RMSE (θ_{or})	RMSE (θ_{opt})
10.4 MHz	2.37°	1.56°	1.96°	1.17°
12.1 MHz	1.94°	1.69°	4.43°	3.40°
10.2 MHz	4.51°	3.23°	1.03°	0.13°

In this way, by jointly measuring the estimated arrival angle and ionospheric reflection virtual height, Equations (1)–(3) can be combined to verify the constraint effect of angle optimization on positioning dispersion, as shown in Figure 11. The positioning results show an approximately elliptical dispersion, indicating that the elevation measurement error plays a dominant role. Compared with the dispersion of positioning points without and after angle optimization, the arrival angle optimization method described in this

paper can effectively converge the positioning. The positioning results of the 10.2 and 10.4 MHz signal radiation sources indicate that the optimized positioning point is closer to the target and even has a higher accuracy compared to the mean positioning directly using the measured angle mean. For the 12.1 MHz signal, it can be observed that the positioning results are significantly concentrated after angle optimization, while the dispersion range of positioning points without angle optimization is extremely large. The overall positioning result also deviates significantly from the true target point. Referring to the ionization diagram in Figure 10b, this may be due to the poor ionospheric reflection at 12.1 MHz, resulting in a low signal-to-noise ratio and causing a significant dispersion of the angle measurement results. This can also be inferred from the angle measurement data shown in Figures 5 and 7. Among the three measurement frequencies, the effective angle pairs of the 12.1 MHz signal are also the lowest, which may lead to some statistical deviation. From the perspective of positioning, the error after optimal selection is slightly larger than the mean positioning result, but the mean positioning point is also included in the optimal set.
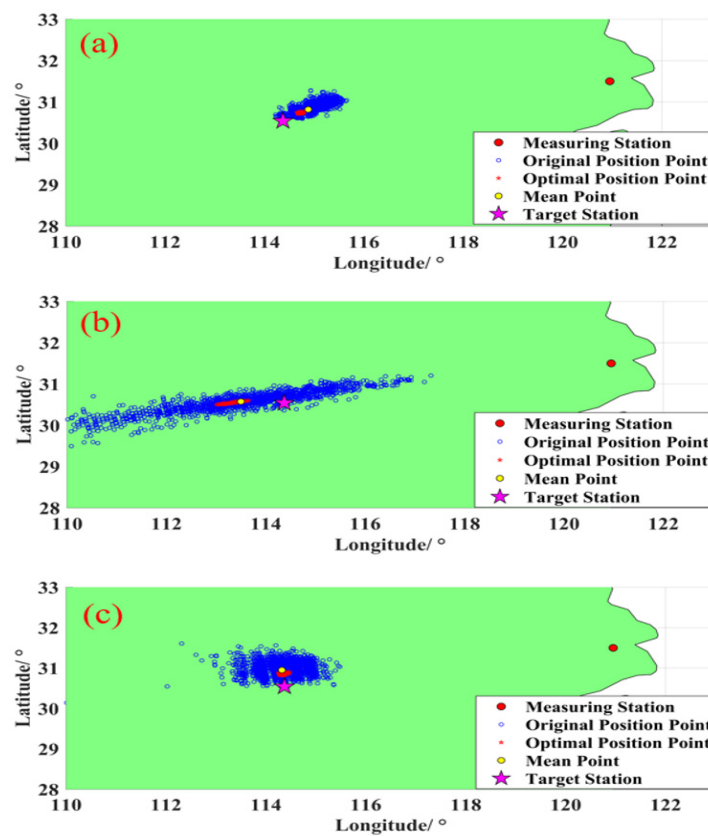
Figure 11. Positioning results: (**a**) positioning results of 10.4 MHz signal; (**b**) positioning results of 12.1 MHz signal; and (**c**) positioning results of 10.2 MHz signal.

It should be pointed out that the positioning results are generally biased towards the north relative to the real target, as pointed out earlier, which may indicate that there may be systematic errors in the baseline pointing of the antenna array. Calibration should be paid attention to in applications.

The ground distance between the positioning point and the target point can be defined as the positioning error ΔD. And, compared to the distance D between the real target point and the measuring station, the relative positioning error can be defined as δ:

$$\delta = \frac{\Delta D}{D} \cdot 100\% \tag{15}$$

Therefore, as shown in the Table 3, statistical data can be further used to evaluate the effectiveness of angle optimization methods in improving positioning accuracy.

Table 3. Positioning error statistical parameters.

Frequency	STD (ΔD_{or})	STD (ΔD_{opt})	δ_{or}	δ_{opt}	δ_{mean}
10.4 MHz	63.91 km	40.97 km	9.07%	6.42%	9.09%
12.1 MHz	194.04 km	102.17 km	22.39%	15.86%	13.14%
10.2 MHz	50.53 km	36.00 km	8.87%	5.64%	7.21%

Where ΔD_{or} and ΔD_{opt} are the positioning errors before and after angle optimization. Their respective standard deviations are statistically analyzed as STD. δ_{or}, δ_{opt}, and δ_{mean}, respectively, represent the relative average errors before and after angle optimization and positioning using the angle mean. For the 10.4 and 10.2 MHz signals, their STDs have decreased to 22.94 km and 14.53 km, respectively. The relative positioning error has also been reduced from 9.07% and 8.87% to 6.42% and 5.64%. Compared to the mean angle position of 9.09% and 7.21%, there is also a significant decrease. Although the positioning effect for 12.1 MHz signals is not very ideal, the STD has also decreased by 91.87 km. The relative positioning error decreased by 6.53% before and after angle optimization. Overall, the angle optimization method proposed in this paper has a significant effect on the dispersion convergence and accuracy improvement of single-station positioning.

5. Conclusions

This paper proposes an angle optimization method to address the issue of significant dispersion in the angle of arrival estimation caused by colored and white noise interference in short-wave single-station positioning. By statistically analyzing the probability density of the angle measurement results and extracting the main peak region, the interference of colored noise was first filtered out. Subsequently, using two-dimensional Gaussian fitting and confidence ellipse bounding, a secondary screening was conducted on the angle measurement results affected by white noise interference. Finally, the results of the positioning experiment proved the convergence and accuracy improvement effect of this method on the dispersion of the single-station positioning results. Although this method inevitably leads to a decrease in real-time performance due to the removal of a large number of angle measurement results, it still has important value for high-time-resolution passive direction-finding programs and stationary or slow-moving targets. At the same time, the positioning results also suggest that attention should be paid to the baseline calibration of antenna arrays and the improvement of the signal-to-noise ratio in applications; otherwise, it may cause system errors or a significant deterioration in positioning accuracy.

Author Contributions: Conceptualization, T.L. (Ting Li) and X.Y.; methodology, T.L. (Tongxin Liu); investigation, T.L. (Ting Li); data curation, G.Y.; writing—original draft preparation, T.L. (Tongxin Liu); writing—review and editing, C.J. and C.L. All authors have read and agreed to the published version of the manuscript.

Data Availability Statement: Data sharing is not applicable to this article.

Conflicts of Interest: The authors declare no conflicts of interest.

References

1. Goodman, J.M. *HF Communication Science and Technology*; Van Nostrand Reinhold: New York, NY, USA, 1991.
2. Guldogan, M.B.; Arıkan, O.; Arıkan, F. A new technique for direction of arrival estimation for ionospheric multipath channels. *Adv. Space Res.* **2009**, *44*, 653–662. [CrossRef]
3. Zheng, L.; Liu, D.; Fei, Y. A novel passive location algorithm based on neural networks. In Proceedings of the IEEE Advanced Information Technology, Electronic and Automation Control Conference (IAEAC), Chongqing, China, 19–20 December 2015; pp. 1124–1127.
4. Gershman, B.A.B. *Array Signal Processing*; IEEE Computer Society: Washington, DC, USA, 2008.
5. Schmidt, R. Multiple emitter location and signal parameter estimation. *IEEE Trans. Antennas Propag.* **1986**, *34*, 276–280. [CrossRef]
6. Roy, R.; Kailath, T. ESPRIT-estimation of signal parameters via rotational invariance techniques. *IEEE Trans. Acoust. Speech Signal Process.* **1989**, *37*, 984–995. [CrossRef]
7. Warrington, E.M. Observations of the directional characteristics of ionospherically propagated HF radio channel sounding signals over two high latitude paths. *IEE Proc.-Microw. Antennas Propag.* **1998**, *145*, 379–385. [CrossRef]
8. Brennan, L.E.; Reed, L.S. Theory of adaptive radar. *IEEE Trans. Aerosp. Electron. Syst.* **1973**, *AES-9*, 237–252. [CrossRef]
9. Jin, L.; In, Q.Y.; Wang, W.J. Time-frequency signal subspace fitting method for direction-of-arrival estimation. In Proceedings of the IEEE International Symposium on Circuits and Systems (ISCAS), Geneva, Switzerland, 28–31 May 2000; Volume 3, pp. 375–378.
10. Chong, Y.; Xie, S.; Huang, T. The bitemporal response function method in studying the ionospheric movement. In Proceedings of the International Symposium on Antennas, Propagation, and EM Theory (ISAPE), Beijing, China, 15–18 August 2000; pp. 548–551.
11. Zhang, X.; Zhao, Z.; Zhang, Y. Investigation of low-latitude ionospheric field-aligned irregularities by oblique backscatter sounding. *IEEE Geosci. Remote Sens. Lett.* **2009**, *7*, 241–245. [CrossRef]
12. Wang, J.; Zhou, X.; Qiao, L.; Gong, W. Application of Wuhan Ionospheric Oblique Backscattering Sounding System (WIOBSS) for the investigation of midlatitude ionospheric irregularities. *Adv. Space Res.* **2018**, *61*, 1254–1259. [CrossRef]
13. Liu, T.; Yang, G.; Hu, Y.; Jiang, C.; Lan, T.; Zhao, Z.; Ni, B. A novel ionospheric sounding network based on complete complementary code and its application. *Sensors* **2019**, *19*, 779. [CrossRef]
14. Zhang, Z.; Wang, W.; Huang, Y.; Liu, S. Decoupled 2-D direction of arrival estimation in L-shaped array. *IEEE Commun. Lett.* **2017**, *21*, 1989–1992. [CrossRef]
15. Ihedrane, M.A.; Bri, S. Direction of arrival using uniform circular array based on 2-D MUSIC algorithm. *Indones. J. Electr. Eng. Comput. Sci.* **2018**, *12*, 30–37. [CrossRef]